TransNav
http://www.transnav.eu
the International Journal
on Marine Navigation
and Safety of Sea Transportation
Volume 19
Number 3
September 2025

DOI: 10.12716/1001.19.03.40

Modelling the Combustion Process of Marine Diesel Engines to Reduce Pollutant Emissions and Influence Vibrations at the Propeller Shaft for a Bulk Carrier Vessel

L.C. Stan
Constanta Maritime University, Constanta, Romania

ABSTRACT: The modeling of the combustion process in internal combustion engines has always been a major concern for experts in the field. The complex nature of the phenomena involved and their strong interdependencies make the approach particularly challenging. The implementation of the provisions outlined in the 1997 Protocol's Annex 6, which aimed at limiting pollutant emissions from ships, especially nitrogen oxides, has been a significant focus for signatory countries since 2010. Coastal areas, particularly those frequented by port technical vessels, have been identified as the most affected regions. From the technical documentation of the ship received on board the ship in the design phase, the following values were calculated: actual diameter of the intermediate shaft 387.2 mm adopting 420 mm, actual bore diameter of 472.4 mm adopting 500 mm, flange thickness coupling 77.4 mm, adopted 100 mm, calculated radius of thread at the base of the 33.6 mm coupling flanges adopted 70 mm, actual diameter of the 46.6 mm flange shaft flange bolts, adopted 64 mm. The ship's propeller has four fixed-pitch blades and a weight of 31.42 tons. Furthermore, torsional vibrations, tree alignment calculations, torsional vibration calculations, critical vibrations, propeller design calculations were calculated in the project. As can be seen from the simulation results, the front-wheel resonance is 155% of the maximum engine speed (127.0 rpm) and the critical resonance is 133% of the maximum engine speed. The result of the spin calculation is therefore acceptable and is not expected to occur at the speed of the engine.

1 INTRODUCTION

The vessel is designed for the transport of the following bulk cargoes: iron ore, grain, coal, phosphates and similar. The vessel is built as a single propeller bulk-carrier with machinery compartment and superstructure at the stern. The ship has a continuous deck with a deckhouse and stern rudder.

The vessel is powered by a supercharged diesel engine, type MAN-B&W 6 S50MC-C reversible with rated power 9480 kW at 127 rpm. The engine is a 6-cylinder, 500 mm bore and 2300 mm stroke. At rated power and with the supercharging system running, the approximate fuel consumption is 173 g/kWh and the oil consumption is 2.25 kg/h.

The main engine is designed to run on heavy fuel (marine diesel) with a maximum viscosity of 3500 sec.Redwood at 380 Centigrade.

Satisfactory torsional vibration behaviour has been found both under normal conditions and when a cylinder is not operating properly. Maximum crankshaft vibration stresses never exceed the limits of the diesel crankshaft. Maximum vibration stresses in the countershaft and propeller are below the guide lines.

The indicated speed range (55~67 rpm) should be achieved against I-6.0 under normal conditions and with one cylinder running rough. In the case of improperly operating one cylinder, engine speed should not exceed 110 rpm (87% of MCR) to avoid resonance of the order of 3.0 and thermal overload of the working cylinders.

The second objective of this paper is to develop a simulation program that can estimate nitrogen oxide emissions produced by compression ignition engines. This idea is based on an analysis of the methods used to implement the regulations specified in Annex 6 of the 1997 Protocol, which focuses on controlling emissions from ships, specifically nitrogen oxides.

The combustion process is undoubtedly the most crucial and complex process occurring in engines. It is responsible for the energy flow used in the engine and is directly linked to all pollutant emissions. Furthermore, the combustion process significantly influences engine efficiency. Despite considerable advancements, the mechanisms of combustion, particularly mixture formation and the chemistry involved, remain complex and not fully understood [1].

The technical characteristics of the ship are:

- IMO number: 9633422;
- Call sign: SVBV2;
- Gross tonnage: 85773;
- TDW: 70434;
- Ship type: Bulk carrier;
- Year of construction: 2014;
- Flag: Greece;
- Construction length: 294.2 meters;
- L between perpendicular: 289 meters;
- Maximum width: 46 meters;
- Construction: Daewoo SB & ME Co., KOR;
- Engine model : 6S50MC-C
- Power at MCR (Kw) : 9480.00
- Speed at MCR (rpm) : 127.00
- Crankshaft : FSB 242456
- Vibration damper : N/A
- Support bearing : M.O.I. = 12249.0 Kg
- Support bearing : M.O.I. = 3539.5 Kg
- Intermediate shaft : D 420.0 / 0.0, UTS = Min. 560 N/mm^2
- Carrier shaft : D 510.0 / 0.0, UTS = Min. 560 N/mm^2
- Propeller : 4-BLADE F.P.propeller

2 PROPULSION SYSTEM SHAFT LINE ANALYSIS

The analysis of the propulsion system's shaft line using the Finite Element Method (FEM) starts with the premise that calculating the exact parameters (displacements, forces) for a continuous structure with complex geometry and boundary conditions is either infeasible or excessively demanding. If an approximate solution that is easier to calculate and reasonably accurate can be obtained, it is considered an acceptable solution for the initial structure. In essence, FEM replaces the structure under analysis with a simplified model that facilitates the calculation of parameters. For structures, FEM can be viewed as an extension of the classical matrix statics method, which was developed for studying assemblies with one-dimensional structural elements (bar structures). FEM enables the analysis of two-dimensional and three-dimensional continuous structures [6].

The process involves discretizing the analyzed structures (either naturally or artificially) and establishing the equilibrium matrix equation for each finite element using a direct formulation (typically represented as a system of algebraic equations). The discrete model's finite elements must be compatible with the structure's spatial development and the mathematical model used to simulate its behavior. For instance, if the structure has a unidirectional development, one-dimensional (1D) finite elements, either straight or curved, are used. In the case of a flat development, two-dimensional (2D) finite elements with straight or curved sides are employed. Similarly, for spatial developments, three-dimensional (3D) finite elements with flat or curved faces are used. In this study, the analysis focuses on the shaft line of a reference ship, which has a total length of 15 m, and the inner diameter is Dint = 0.4 · Dext. The shaft construction is simple, without flanges.

The shaft model is generated using specialized software such as Ansys, which is designed for finite element analysis. Subsequently, the following operating scenarios are analyzed: operating the engine at maximum power and locking the propeller in situations such as landing on a sandbank, as well as the normal operating mode of the propulsion system when the ship reaches a maximum speed of 15 knots (Nd), a speed corresponding to the maximum power of the propulsion engine.

Additionally, the simulation considers the pushing force at its maximum value. To initiate the simulation process, the measurement units for the precise determination of shaft line parameters are established. Geometric parameters, such as length along the X, Y, Z axes, volume, mass, scaling factor, number of bodies, number of active bodies, and type of analysis (in this case, three-dimensional), are introduced. Subsequently, the Ansys program automatically generates the geometric model of the shaft:

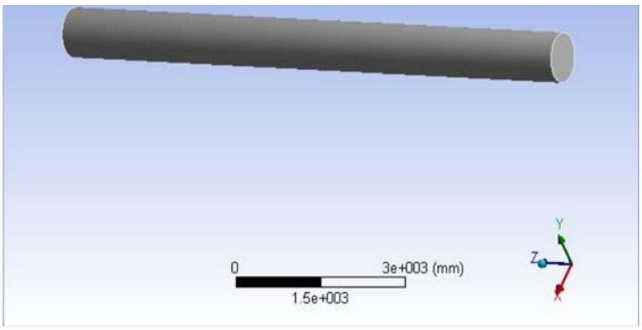

Figure 3. Generating the shaft geometric model [5]

The next step involves defining the coordinate system and setting parameters for generating the discretized model of the shaft. Once the model is generated, the shaft's discretization is performed using square finite elements [5].:

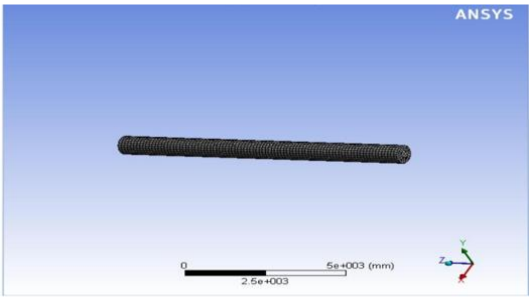

Figure 4. Performing shaft discretization using square finite elements [5]

The analyzes can then be performed on the defined and discretized model of the shaft. As in the previous steps, a series of parameters are redefined and then loads related to the motor torque are applied:

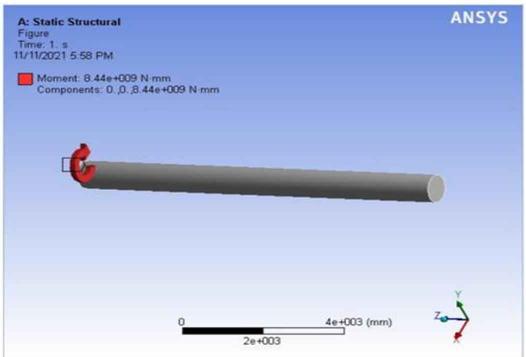

Figure 5. Applying loads related to the motor torque on the shaft [5]

The specified torque given by the engine depends on the parameters for the analysis of total, directional, stress deformations are defined below, as shown in the figures below:

TABLE 11
Model (A4) > Static Structural (A5) > Solution (A6) > Results

Object Name	*Total Deformation*	*Directional Deformation*	*Equivalent Elastic Strain*	*Equivalent Stress*	*Strain Energy*
State	Solved				
Scope					
Scoping Method	Geometry Selection				
Geometry	All Bodies				
Definition					
Type	Total Deformation	Directional Deformation	Equivalent Elastic Strain	Equivalent (von-Mises) Stress	Strain Energy
By	Time				
Display Time	Last				
Calculate Time History	Yes				
Identifier					
Suppressed	No				
Orientation		X Axis			
Coordinate System		Global Coordinate System			
Results					
Minimum	0. mm	-9.4269 mm	6.4773e-005 mm/mm	9.258 MPa	1977.1 mJ
Maximum	9.43 mm	9.4267 mm	6.4371e-004 mm/mm	128.31 MPa	42016 mJ
Information					
Time	1. s				
Load Step	1				
Substep	1				
Iteration Number	1				
Integration Point Results					
Display Option			Averaged		

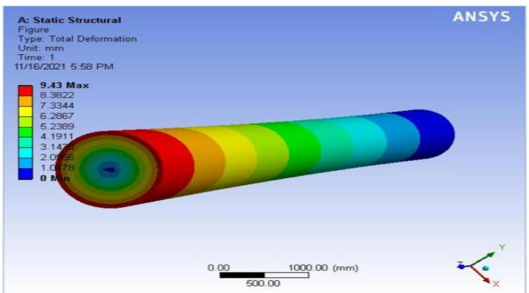

Figure 9. Diagram of total deformations expressed in [mm] [5]

2.1 *Natural frequencies and resonance modes*

At the end of the analysis the program automatically generates a series of tables in which data are presented regarding the qualities of the material from which the shaft line is produced and how it behaves during the simulation.

Table 1.

Module no.	1	2	3
Frequency (Cpm)	362.9	1356.5	2775.3
Nr	Vibration modes		
1	- 0.8066	- 0.7925	- 0.5072
2	- 0.7897	- 0.5603	0.1150
3	- 0.7653	- 0.2492	0.7282
4	- 0.7352	0.0860	1.0000
5	- 0.6981	0.4214	0.8062
6	- 0.6565	0.7020	0.2448
7	- 0.6116	0.8968	- 0.4022
8	- 0.5737	0.9733	- 0.7613
9	- 0.5473	1.0000	- 0.9211
10	0.5168	0.2915	- 0.3440
11	1.0000	- 0.0507	- 0.0126

Module no.	1	2	3
Frequency (Cpm)	362.9	1356.5	2775.3
Nr.	Moment of inertia (Knm)		
1	$- 0.144 \cdot 10^5$	$- 0.197 \cdot 10^6$	$- 0.529 \cdot 10^6$
2	$- 0.194 \cdot 10^5$	$- 0.247 \cdot 10^6$	$- 0.487 \cdot 10^6$
3	$- 0.242 \cdot 10^5$	$- 0.269 \cdot 10^6$	$- 0.218 \cdot 10^6$
4	$- 0.288 \cdot 10^5$	$- 0.261 \cdot 10^6$	$0.151 \cdot 10^6$
5	$- 0.332 \cdot 10^5$	$- 0.224 \cdot 10^6$	$0.448 \cdot 10^6$
6	$- 0.374 \cdot 10^5$	$- 0.162 \cdot 10^6$	$0.539 \cdot 10^6$
7	$- 0.412 \cdot 10^5$	$- 0.832 \cdot 10^5$	$0.390 \cdot 10^6$
8	$- 0.429 \cdot 10^5$	$- 0.433 \cdot 10^5$	$0.260 \cdot 10^6$
9	$- 0.458 \cdot 10^5$	$0.305 \cdot 10^5$	$- 0.248 \cdot 10^5$
10	$- 0.456 \cdot 10^5$	$0.323 \cdot 10^5$	$- 0.336 \cdot 10^5$

Table 2. Engine resonance speed and vector summation

Order	Natural frequency (Cpm)		
	362.9	1356.5	2775.3
1.0	363/ 0.035	1356/ 0.176	2775/ 1.817
2.0	181/ 0.155	678/ 1.084	1388/ 0.352
3.0	121/ 0.410	452/ 3.059	925/ 1.194
4.0	91/ 0.155	339/ 1.084	694/ 0.352
5.0	73/ 0.035	271/ 0.176	555/ 1.817
6.0	60/ 5.390	226/ 1.446	463/ 2.492
7.0	52/ 0.035	194/ 0.176	396/ 1.817
8.0	45/ 0.155	170/ 1.084	347/ 0.352
9.0	40/ 0.410	151/ 3.059	308/ 1.194
10.0	36/ 0.155	136/ 1.084	278/ 0.352
11.0	33/ 0.035	123/ 0.176	252/ 1.817
12.0	30/ 5.390	113/ 1.446	231/ 2.492
13.0	28/ 0.035	104/ 0.176	213/ 1.817
14.0	26/ 0.155	97/ 1.084	198/ 0.352
15.0	24/ 0.410	90/ 3.059	185/ 1.194
16.0	23/ 0.155	85/ 1.084	173/ 0.352
17.0	21/ 0.035	80/ 0.176	163/ 1.817
18.0	20/ 5.390	75/ 1.446	154/ 2.492
19.0	19/ 0.035	71/ 0.176	146/ 1.817
20.0	18/ 0.155	68/ 1.084	139/ 0.352

Stress value : 83.5 N/mm^2
Speed : 60.5 rpm
No. of shafts : 9

Table 3. Table with maximum stress data (N/mm²)

RPM	1	2	3	4	5	6	7	8	9	10
82	3.8	7.9	8.9	6.6	10.6	9.9	2.6	2.9	10.5	5.9
84	4.3	9.0	9.9	7.2	11.4	10.4	2.8	3.0	10.3	5.7
86	5.0	9.6	10.0	8.0	11.9	10.2	3.1	3.2	10.6	5.9
88	5.4	10.0	10.3	8.8	12.6	10.4	3.5	3.5	11.7	6.5
90	7.5	12.2	13.4	12.2	15.3	11.8	5.0	4.6	13.3	7.5
82	6.3	12.0	12.3	10.3	13.5	10.1	4.2	4.0	12.1	6.8
94	5.2	11.0	11.7	8.9	12.2	9.3	3.2	3.2	11.1	6.2
96	5.6	11.0	12.6	9.2	11.9	10.0	3.0	2.9	9.9	5.5
98	5.5	11.0	12.1	8.7	12.1	10.9	2.7	2.7	9.2	5.1
100	4.8	11.0	11.4	8.1	12.4	11.1	2.2	2.5	8.8	4.9
102	4.7	11.3	11.5	7.9	12.8	11.1	2.0	2.3	8.6	4.8
104	4.8	11.7	11.9	8.0	13.1	11.4	2.0	2.3	8.4	4.7
106	5.1	12.7	12.9	8.6	14.0	12.3	2.1	2.3	8.6	4.8
108	5.1	12.7	12.9	8.6	14.0	12.3	2.1	2.3	8.6	4.8
110	5.3	12.8	13.3	8.9	14.6	13.0	2.3	2.4	8.8	4.9
112	6.4	14.7	15.6	10.5	16.3	14.4	3.0	2.8	9.8	5.5
114	6.5	14.3	15.4	11.1	17.3	15.2	3.6	3.1	10.7	6.0
116	5.9	13.7	14.8	10.3	16.9	14.8	4.0	3.7	15.2	6.8
118	5.9	14.4	15.4	10.4	16.9	14.8	4.9	4.7	15.4	8.6
120	6.5	15.2	16.5	10.8	16.4	14.8	5.4	5.5	18.7	10.4
122	6.7	15.3	16.9	10.0	15.9	14.9	4.9	5.2	18.7	10.4
124	6.5	15.0	16.6	9.2	16.1	15.4	4.4	4.6	15.9	8.9
126	6.2	15.3	16.6	9.2	16.4	15.9	4.0	4.1	14.2	7.9
128	6.2	15.6	16.9	9.7	16.9	16.1	3.6	3.5	12.7	7.1
130	6.6	15.9	17.5	10.3	17.2	16.4	3.4	3.1	11.2	6.3
132	7.5	16.6	18.5	11.3	17.7	17.0	3.3	2.8	10.2	5.7
134	9.0	18.6	20.5	13.2	18.3	18.1	3.7	2.8	9.7	5.5
136	10.8	20.8	21.6	14.8	20.6	18.0	3.9	2.6	10.0	5.7
138	10.1	18.9	18.5	13.0	19.8	16.4	3.2	2.2	9.0	5.1
140	9.6	18.0	17.6	12.3	20.3	16.4	3.1	2.0	8.3	4.7

The values with a negative sign are the vibratory torques (kNm)
Engine type : 6S50MC-C
Tuning wheel : 12249.0 kgm²
MCR rating : 9480 kW × 127 rpm
Turning wheel : 3539.5 kgm²
Combustion conditions : Normal combustion
Gas harmonics : 242503
Speed range limit : 55 ~ 67 RPM
Limit : Diesel engine crankshaft limits
Crankshaft : FSB 242456 / SOLID CRANK PIN

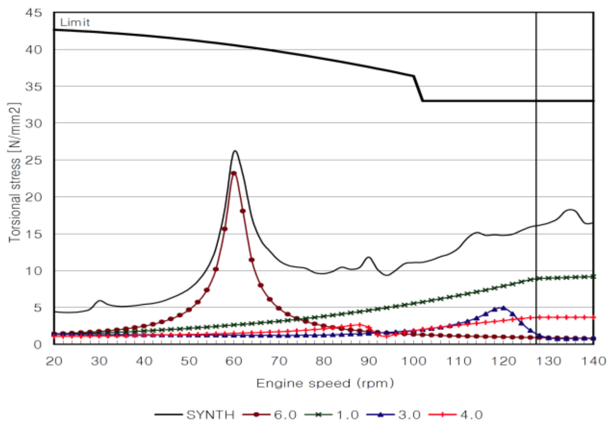

Figure 10. Torsional vibration stress of crankshaft No.6 DIA. = 600.0 mm UTS = 610.0 N/mm²

Limit tau1 : Limit for continuous fuctioning with factor 1.0 Ck

Limit tau2 : Limit for transient operation

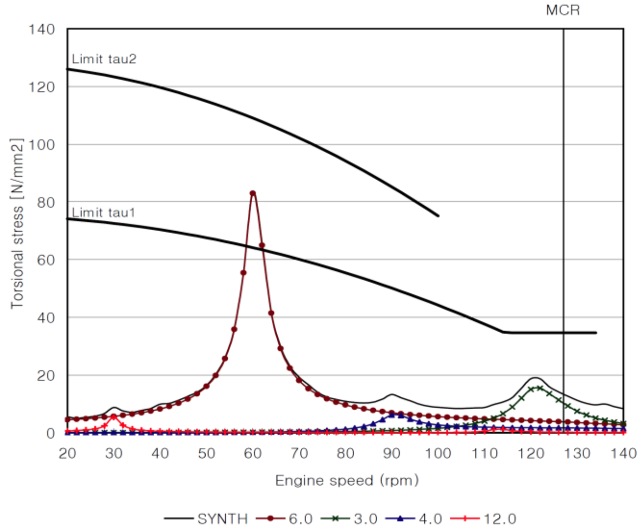

Figure 11. Torsional vibration stress of intermediate shaft No. 9. DIA. = 420.0 mm UTS = 560.0 N/mm²

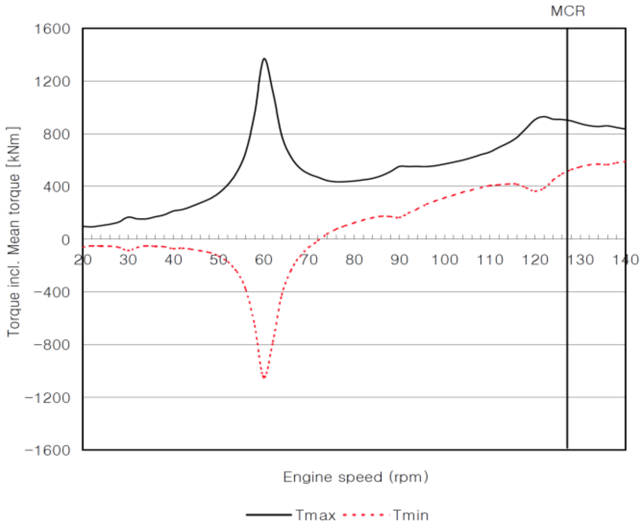

Figure 12. Maximum and minimum torque. Average torque of the carrier shaft 10

Speed range limit : 55 ~ 67 RPM
Maximum speed : ~ 110 rpm (Misfiring only)
Limit : Diesel crankshaft limits
Crankshaft : FSB 242456 / SOLID CRANK PIN

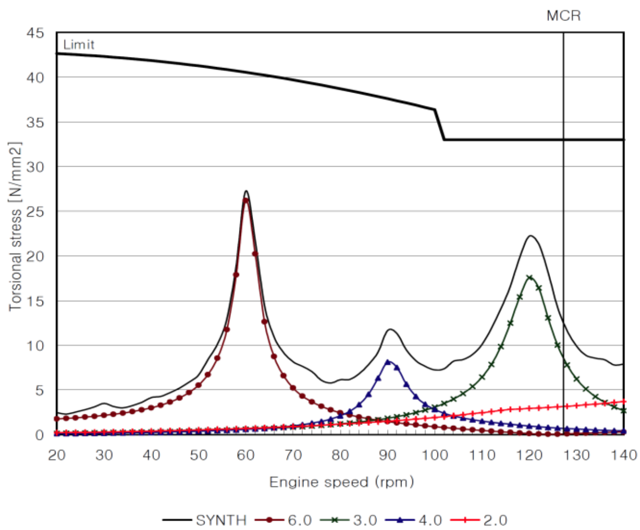

Figure 13. Torsional vibration stress of crankshaft No. 7. DIA. = 600.0 mm UTS = 610.0 N/mm²

The alignment calculation for the shaft system was performed using the Nauticus Shaft Aligment program. The shaft alignment procedure is followed the standard shipyard procedure. Verification of the shaft alignment results shall be carried out according to standard shipyard methods. (Gap & SAG, jacking, etc.)

The purpose of this shaft alignment calculation is to find a set of vertical offsets for the intermediate shaft bearings and engine bearings to ensure that the bearing loads are kept within limits for all bearings.

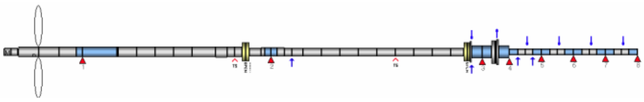

Figure 14. Shaft alignment

Material data

Material data	Conditions	E-MOD (N/m²)	Density (kg/m³)
1	In the air	2.10 · 1011	7 850
2	In the see water	2.10 · 1011	6 850
3	In fresh water	2.10 · 1011	7 000
4	Unweighability	2.10 · 1011	0

Propeller weight:
50% submerged (half submerged) : 16.347 kg - 1.102 kg = 15.245 kg
Propeller weight in air : 16,347 kg
Propeller weight half submerged : 1/2 × 16.347 kg / 7.600g/cm³ × 1.025g/cm³ = 1.102 kg
75% submerged : 16.347 kg - 1.653 kg = 14.694 kg
100% Immersed (Totally submerged) : 16,347 kg - 2,205 kg = 14,142 kg

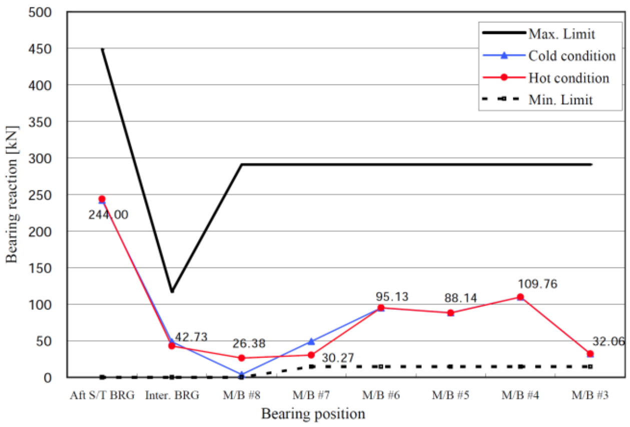

Figure 15. Graphical results of the loading of the pens

The calculation is conducted at maximum speed and power, with an engine speed of 2400 rpm, effective power of 48 kW, specific consumption of 238.077 g/kWh, and an effective injection advance of β = 5.5°RAC (rotation angle of the crankshaft). The program performs an engine cycle starting at 120 °RAC before the inner neutral point (INP). At this point, it is assumed that turbulence in the cylinder ensures uniform velocity gradients, resulting in approximately uniform velocity within the cylinder. The program utilizes 12 modes, and the fuel considered is saturated pure hydrocarbon $C_{10}H_{20}$. The reactions are divided into four slow kinetic reactions (fuel oxidation and the extended Zel'dovich mechanism for nitrogen oxide formation) and eight equilibrium reactions (element dissociation reactions). The injection advance is set to 5.5 °RAC, and the injection duration is 17 degrees. The average Sauter diameter (DSM) is set to $1x10^{-3}$ cm. The discretization network comprises 624 nodes and 583 cells. The size of the discretization network can be adjusted using a set of parameters. Comparative values of pressure and temperature, both calculated and measured, are depicted in Figure 16 [2].

The simulation process requires 36 hours and 23 minutes of computation time for the given discretization network, which includes 624 computing cells and 1230 drop packets. The maximum amount of working memory required is 425 MB. The output data is stored in 2153 text files (one file for every 0.1°RAC), occupying 682 MB of hard disk storage.

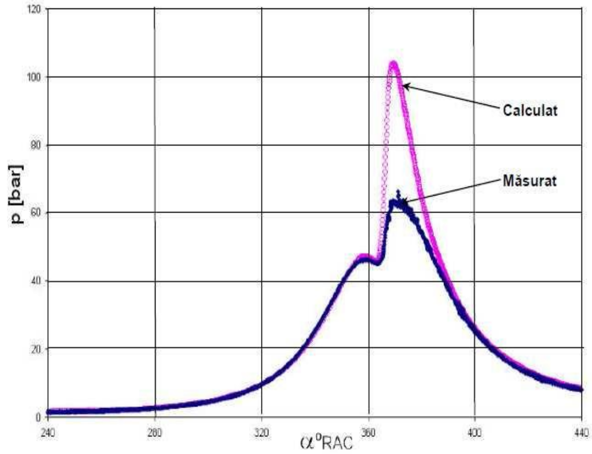

Figure 16. Indicated pressure

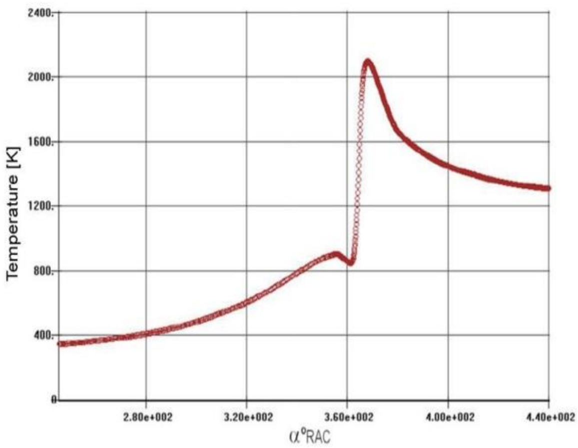

Figure 17. Cycle average temperature

The results obtained from the specific files are processed using a program written in Matlab, and the resulting graphs are presented below. Due to the large dimensions of the tables with values, which lack practical relevance, only the commentaries on each chart are provided. Figure 16 shows a comparison between calculated and experimentally measured pressure values per cycle [3].

The calculated and measured pressures show good agreement, with the exception of the combustion period, during which the calculated pressure is significantly higher than the measured one. This disparity is expected to some extent, given the combustion model used and the discretization scheme employed. The scientific literature includes numerous examples of simulations performed with similar models (e.g., KIVA I, Conchas-Spray), which have highlighted similar issues. Due to this discrepancy, it is anticipated that other quantities will be affected, particularly the emissions of nitrogen oxides.

Some results are provided below to demonstrate the program's capabilities.

The calculated average temperature within the cylinder is presented, where the calculated temperature represents the mass average of temperatures in the computing cells for each time step.

The maximum pressure per cycle affects the temperature, leading to a sharp increase in nitrogen oxide concentrations [4].

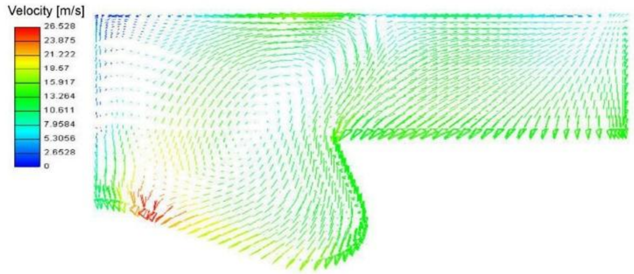

Figure 18.Velocity distribution in the cylinder for 400°RAC[5]

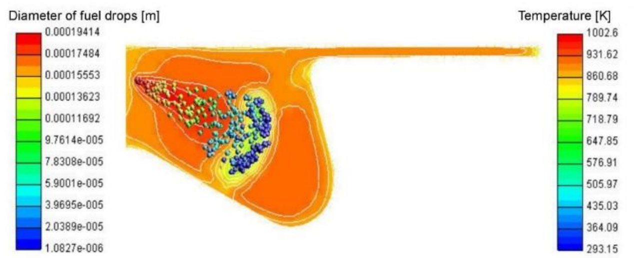

Figure 19. Fuel jet at 357 °RAC and 2 °RAC, after injection start[5]

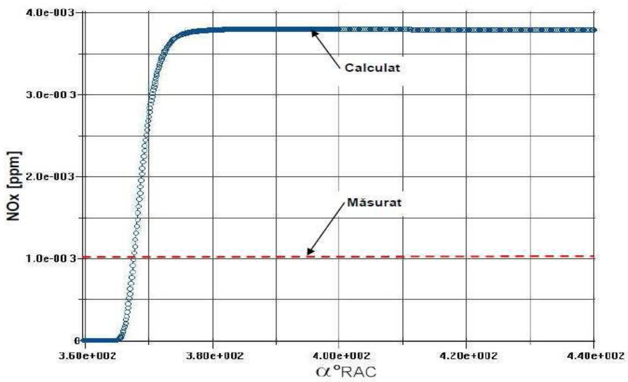

Figure 20. Evolution of NOx concentration in the cylinder, during one cycle

Figure 20 shows the evolution of the NOx concentration in the cylinder over a cycle calculated using the program and the experimentally measured average value. As expected, there are big differences. The maximum pressure per cycle influenced the temperature, which caused a sharp increase in the concentration of nitrogen oxides [6].

From the analysis of the results, it can be seen that, for the combustion process, the obtained results have only a qualitative character, these obtained values not being in accordance with the measured values. Instead, the evolution of the phenomena (as they are described in the literature for similar cases) inside the cylinder is captured with sufficient accuracy. Thus, one may notice:

- vortices created by the fuel jet,
- the effect of the combustion chamber in the piston head which:
- concentrates, in the first phase of the combustion process, hot gases, having high concentrations of fuel vapors and low concentrations of oxygen, preventing the formation of NOx;
- in the second phase, the hot gases come out strongly turbulent from the
- combustion chamber and mix with the air from the upper dead sap, maintaining a high temperature and pressure;
- the presence of flame at the periphery of the fuel jet in the envelope, where the mixtures have concentrations close to the stoichiometric ones;
- NOx formation in areas with high temperatures and poor mixtures at the periphery of the jet;
- the presence of vortices at the exit of the rich mixtures from the combustion chamber, from the piston head, vortices that prevent the uniformity of the mixtures;
- the presence of areas on the wall with low temperatures and areas without mixing, where, depending on the flow regime, unused air may remain.

Apart from the limitations imposed by the adopted models, presented in the theoretical substantiation, there are other problems related to the numerical solution of the system of differential equations, which do not exactly meet all the requirements (as far as they are known) of stability and convergence.

Some known problems in the literature, frequently encountered in the case of internal combustion engines, were also highlighted for the case under consideration.

Due to the obtained high pressures, other results, as expected, were altered, among them being the emissions of nitrogen oxides, which had values much higher than the measured ones.

As the proposed algorithm is based on the implicit calculation of the pressure, its value being

used to update the other parameters, it goes without saying that it is necessary to implement algorithms designed to reduce it to acceptable and realistic values.

This approach was also preferred due to the experimental database, so that the pressure is the only quantity for which the instantaneous values in the cycle are known, and the other measured quantities being averaged over several cycles [7].

3 CONCLUSIONS

The results obtained in this study have a qualitative nature, as the values do not perfectly align with the measured ones. However, the evolution of phenomena inside the cylinder is captured with sufficient accuracy. This includes the vortices created by the fuel jet, the impact of the combustion chamber on the piston head, the presence of flame at the periphery of the fuel jet in the tire, the formation of nitrogen oxides in high-temperature areas and lean mixtures at the jet's periphery, and the presence of vortices at the outlet of rich mixtures from the combustion chamber into the piston head. Furthermore, areas on the wall with low temperatures and areas without a direct connection to the combustion chamber are identified. These results allow for an improved understanding of the combustion process and the subsequent emission formation mechanisms. Future studies should focus on refining the combustion model, especially during the combustion period, where the measured pressure values differ from the calculated ones. Additionally, a more detailed analysis of nitrogen oxide formation should be performed to accurately predict emission levels. To achieve this, additional mechanisms should be included in the combustion model to account for thermal and prompt mechanisms, as well as the impact of turbulence on flame structure. The study is limited by the available computational resources, which restricted the resolution of the discretization network and the simulation duration.

As can be seen from the results, the forward spin resonance is 155% of the maximum engine speed (127.0 rpm) and the critical resonance is 133% of the maximum engine speed. The result of the rotation calculation is therefore acceptable and is not expected to show engine speed.

Also, from the mathematical model that the forward spin resonance is 155% of the maximum engine speed (127.0 rpm) and the critical resonance is 133% of the maximum engine speed. The result of the rotation calculation is therefore acceptable and no engine speed variations are expected to occur.

REFERENCES

[1] SABĂU A., BUZBUCHI N., ŞOLOIU V. A., Combustion Numerical Modelling in Diesel Engines, the 11th National Conference for Thermotechnics, Galaţi, (2001).

[2] SABĂU A., BUZBUCHI N., ŞOLOIU V. A., Combustion Processs Simulation, Analele Universităţii ”Ovidius”, Constanța, (2000).

[3] SABĂU A., BUZBUCHI N., SABIE, S., Modelarea jetului axisimetric, Analele Universităţii Maritime din Constanța, Constanța, (2003).

[4] FAITAR C., NEDELCU A.T., BUZBUCHI N., STAN L., DUMITRACHE L. M. Considerations of the energy balance of an internal combustion engine and the recovery of heat lost through the cooling water, IOP Conference Series: Materials Science and Engineering, ModTech 2019, https://iopscience.iop.org/article/10.1088/1757-899X/591/1/012088/meta , (2019)..

[5] ANSYS.

[6] WIESER K., VERSAEVEL P., MOTTE, P., A New 3D Model for Vaporizing Diesel Sprays Based on Mixing-Limited Vaporization, SAE 2000-01-0949, DOI: https://doi.org/10.4271/2000-01-0949 2000.

[7] BUZBUCHI N., STAN L.C., FAITAR C., Dynamic behavior modeling and simulation of marine propulsion systems, Editura NAUTICA, ISBN 987-606-681-170-5, Constanta, (2022).